# Calculation of Dynamic Motions and Tensions in Towed Underwater Cables

Franz S. Hover, Mark A. Grosenbaugh, and Michael S. Triantafyllou

*Abstract*— **A matrix method for mooring system analysis is extended to address the dynamic response of towed underwater systems. Key tools are equivalent linearization and small perturbation theory, and a pitching towfish model. Two examples of application of the technique are provided. The first studies a fundamental limitation to constrained passive heave compensation, while the second concerns the use of floated tethers as a means for dynamic decoupling.**

*Index Terms*—**Cable dynamics, ocean towing, wave excitation.**

## I. Introduction

THE DESIGN OF A towed underwater system is often constrained by the dynamic tensions and deflections induced by motions of the surface vessel in heavy weather. A towed system has a nonlinear response because of large curvatures and quadratic fluid drag, so either lengthy simulation or an approximate analysis is required. Two major simplifications are common: small perturbations and equivalent linearization. In the former, dynamic deflections are considered as small motions from a static configuration whose shape is known [14], [13], [20]. Retaining only first-order terms then renders the geometric coupling terms linear. Perturbation theory works especially well for ocean systems because static cable curvatures can be quite large, while the wave-induced motions are comparatively small. Equivalent linearization is a standard technique in nonlinear mechanics [15]; the linearization of fluid drag has been widely used in ocean applications, enabling approximate frequency-domain analysis [16], [17].

Based on these simplifications, a matrix method for mooring system analysis has been developed by Bliek [1], [8]. This method uses an iterative loop to tune the linearizations, and involves transfer matrices that arise from a finite-difference decomposition of the cable equations.

The present paper develops an extension of Bliek's method to the towing of a submerged towfish. Like the original form, we consider only two-dimensional, single-line systems, although it will become apparent in the sequel that more complicated configurations are possible if the transfer matrices are cascaded. This flexibility, coupled with the inherent computational speed of the method, make the algorithm an attractive design tool.

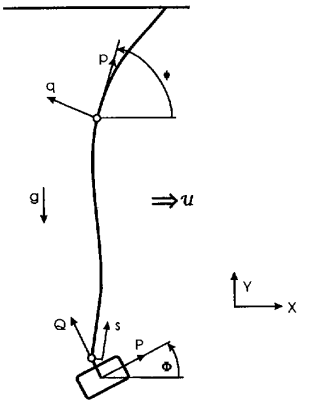


Fig. 1. Orientation and nomenclature for a generic towfish system.

The paper includes several detailed examples which illustrate the usefulness of the approach. In the first, we consider the optimization problem of picking physical parameters for a passive heave compensator. In particular, a fundamental tradeoff occurs when the motions of the compensator (with respect to the vessel) are physically limited. Our analysis indicates that in high seas, the best result may in fact be obtained by locking the compensator.

The second example concerns the use of static cable shaping to isolate a remotely-operated vehicle (ROV) from wave excitations. More specifically, we investigate adding floats to a neutral cable to achieve a static "$S$-shape," which decouples motions at the forced end from those at the other.

## II. Development of Linearized Equations

### A. Cable Statics and Dynamics

The equations of motion for cables have been worked out in two and three dimensions by many authors, e.g., [12], [22], [10]. For the purposes here, we assume that the effects of torsion, rotational inertia, and bending stiffness are negligible. Then the two-dimensional governing equations in still water are given as follows (see Table I and Fig. 1 for nomenclature):

$$m\left(\frac{\partial u}{\partial t} - \frac{\partial \phi}{\partial t}v\right) = \frac{\partial T}{\partial s} - w_0 \sin\phi - \frac{1}{2}\rho d C_t u|u| \tag{1}$$

$$m\left(\frac{\partial v}{\partial t} + \frac{\partial \phi}{\partial t}u\right) + m_a \frac{\partial v}{\partial t} = T\frac{\partial \phi}{\partial s} - w_0 \cos\phi - \frac{1}{2}\rho d C_d v|v| \tag{2}$$

Manuscript received April 1993; revised November 1993. This work was supported by the ONR under Contracts N00014-90-J-1912 and N00014-89-J-3061, and by the Packard Foundation.

F. S. Hover is with the Monterey Bay Aquarium Research Institute, Pacific Grove, CA 93950.

M. A. Grosenbaugh is with the Deep Submergence Laboratory, Woods Hole Oceanographic Institution, Woods Hole, MA 02543.

M. S. Triantafyllou is with the Department of Ocean Engineering, Massachusetts Institute of Technology, Cambridge, MA 02139.

IEEE Log Number 9401466.

0364–9059/94$04.00 © 1994 IEEE

TABLE I
NOMENCLATURE

| | |
|---|---|
| cable length | $L$ |
| cable diameter | $d$ |
| cable water weight/length | $w_o$ |
| cable mass/length | $m$ |
| cable added mass (lateral)/length | $m_a$ |
| water density | $\rho$ |
| cable normal, tangential drag coefficient | $C_d$, $C_t$ |
| cable elasticity | $E$ |
| towfish air weight | $W$ |
| towfish buoyant force | $B$ |
| mass of towfish | $M$ |
| added mass of towfish; $P$-, $Q$-direction | $M_{aP}$, $M_{aQ}$ |
| effective rotational inertia of towfish | $J$ |
| drag coefficient of towfish | $C_{d,t}$ |
| area of towfish face; $P$-, $Q$-direction | $A_P$, $A_Q$ |
| length of towfish | $l$ |
| added mass center in body coordinates | $r_{aP}$, $r_{aQ}$ |
| buoyancy center in body coordinates | $r_{bP}$, $r_{bQ}$ |
| towpoint location in body coordinates | $r_{cP}$, $r_{cQ}$ |
| drag center in body coordinates | $r_{dP}$, $r_{dQ}$ |
| apparent mass of heave compensator | $m_{comp}$ |
| apparent damping of heave compensator | $b_{comp}$ |
| apparent stiffness of heave compensator | $k_{comp}$ |
| depth-dependent current | $\mathcal{U}(Y)$ |
| lagrangian cable coordinate | $s$ |
| cable tension | $T(s,t)$ |
| cable pitch angle | $\phi(s,t)$ |
| cable tangential deflection, velocity | $p(s,t)$, $u(s,t)$ |
| cable normal deflection, velocity | $q(s,t)$, $v(s,t)$ |
| towfish longitudinal deflection, velocity | $P(t)$, $U(t)$ |
| towfish lateral deflection, velocity | $Q(t)$, $V(t)$ |
| towfish pitch angle | $\Phi(t)$ |
| standard deviation of random variable $z(t)$ | $\sigma_z$ |
| average $1/n$th highest value of random variable $N$ height (exception: $T_{1/n}$ is average $1/n$th tension amplitude) | $N_{1/n}$ |
| wave amplitude | $H(t)$ |
| vessel heave amplitude | $D(t)$ |
| vessel-relative motion of cable top | $R(t)$ |

The required compatibility relations may be expressed in terms of velocities as follows:

$$\frac{\partial u}{\partial s} - \frac{\partial \phi}{\partial s} v = \frac{\partial \epsilon}{\partial t} \tag{3}$$

$$\frac{\partial v}{\partial s} + \frac{\partial \phi}{\partial s} u = \frac{\partial \phi}{\partial t}. \tag{4}$$

We use the standard constitutive law that strain $\epsilon = T/EA$.

In order to separate the static and dynamic problems, we invoke the expansion $T \simeq \bar{T} + \tilde{T}$, where $\bar{T}$ is the static tension, and $\tilde{T}$ is the dynamic tension. Similarly, $\phi \simeq \bar{\phi} + \tilde{\phi}$. To compute the static configuration in the presence of a current $\mathcal{U}(Y)$ (we drop the argument in the sequel), a drag model is needed. For example, a form that uses the decomposed velocity vector is

$$p - \text{drag: } \frac{1}{2}\rho d C_t \mathcal{U} \cos\bar{\phi} |\mathcal{U} \cos\bar{\phi}| \left(1 + \frac{\bar{T}}{2EA}\right), \tag{5}$$

$$q - \text{drag: } -\frac{1}{2}\rho d C_d \mathcal{U} \sin\bar{\phi} |\mathcal{U} \sin\bar{\phi}| \left(1 + \frac{\bar{T}}{2EA}\right). \tag{6}$$

These hydrodynamic forces have the standard Morison form, and account for both an elongation and a decrease in diameter through Poisson's ratio $\nu = 0.5$. This value is typical for synthetic cables which preserve their volume under stretching.

The resulting dynamic equations in a current $\mathcal{U}$ may now be derived. The expanded forms of $T$ and $\phi$ are inserted into the governing equations, the static terms subtracted out, and the small-angle assumption applied to $\tilde{\phi}$. Also we neglect coupled nonlinear terms higher than first order; this enables us to replace $u$ with $\frac{\partial p}{\partial t}$ and $v$ with $\frac{\partial q}{\partial t}$. The resulting equations of motion are expressed as displacements, giving a more natural framework for dynamic response studies:

$$\begin{aligned}\frac{\partial \tilde{T}}{\partial s} &= m\frac{\partial^2 p}{\partial t^2} + w_0 \cos\bar{\phi}\tilde{\phi} \\ &\quad + \frac{1}{2}\rho d C_t \left(\frac{\partial p}{\partial t} - \mathcal{U}\cos\bar{\phi}\right)\left|\frac{\partial p}{\partial t} - \mathcal{U}\cos\bar{\phi}\right|\left(1 + \frac{\bar{T}}{2EA}\right) \\ &\quad + \frac{1}{2}\rho d C_t \mathcal{U}\cos\bar{\phi}|\mathcal{U}\cos\bar{\phi}|\left(1 + \frac{\bar{T}}{2EA}\right),\end{aligned} \tag{7}$$

$$\begin{aligned}\bar{T}\frac{\partial \tilde{\phi}}{\partial s} &= -\tilde{T}\frac{\partial \bar{\phi}}{\partial s} + (m + m_a)\frac{\partial^2 q}{\partial t^2} - w_0 \sin\bar{\phi}\tilde{\phi} \\ &\quad + \frac{1}{2}\rho d C_d \left(\frac{\partial q}{\partial t} + \mathcal{U}\sin\bar{\phi}\right)\left|\frac{\partial q}{\partial t} + \mathcal{U}\sin\bar{\phi}\right|\left(1 + \frac{\bar{T}}{2EA}\right) \\ &\quad - \frac{1}{2}\rho d C_d \mathcal{U}\sin\bar{\phi}|\mathcal{U}\sin\bar{\phi}|\left(1 + \frac{\bar{T}}{2EA}\right).\end{aligned} \tag{8}$$

Since the small angle assumption has been made, the compatibility equations ((3) and (4)) no longer need to apply for arbitrary dynamic angles. In this case they are entirely equivalent to relations derived using displacements:

$$\frac{\partial p}{\partial s} = \frac{\tilde{T}}{EA} + q\frac{\partial \bar{\phi}}{\partial s}, \tag{9}$$

$$\frac{\partial q}{\partial s} = \tilde{\phi}\left(1 + \frac{\bar{T}}{EA}\right) - p\frac{\partial \bar{\phi}}{\partial s}. \tag{10}$$

Adopting linear damping coefficients, $b_p(s)$ and $b_q(s)$, which are to be found iteratively, the governing equations and compatibility relations can be written in the frequency domain in matrix form, as shown at the bottom in (11) [1] or $\frac{d\vec{y}}{ds} = A(s)\vec{y}$. The time-constant terms in (7) and (8) transform to a delta function, so they have no bearing on the frequency response. Following Bliek, the cable is discretized into $n$ nodes, numbered "1" at the towfish connection point, and "$n$" at the surface point, where there is an imposed motion. The unstretched distance between nodes is taken as $ds$, and the

$$\frac{d}{ds}\begin{bmatrix}\tilde{T}\\ \tilde{\phi}\\ p\\ q\end{bmatrix} = \begin{bmatrix}0 & w_0\cos\bar{\phi} & -m\omega^2 + i\omega b_p(s) & 0\\ -\frac{1}{\bar{T}}\frac{\partial\bar{\phi}}{\partial s} & -\frac{w_0\sin\bar{\phi}}{\bar{T}} & 0 & \frac{1}{\bar{T}}(-(m+m_a)\omega^2 + i\omega b_q(s))\\ \frac{1}{EA} & 0 & 0 & \frac{\partial\bar{\phi}}{\partial s}\\ 0 & 1 + \frac{\bar{T}}{EA} & -\frac{\partial\bar{\phi}}{\partial s} & 0\end{bmatrix}\begin{bmatrix}\tilde{T}\\ \tilde{\phi}\\ p\\ q\end{bmatrix} \tag{11}$$

evolution of $\vec{y}$ on the length can then be written as follows:

$$\frac{\vec{y}_{i+1}-\vec{y}_i}{ds} \simeq \frac{A(s_{i+1})\vec{y}_{i+1}+A(s_i)\vec{y}_i}{2} \Longrightarrow$$

$$\vec{y}_{i+1} \simeq \left[I-\frac{ds}{2}A(s_{i+1})\right]^{-1}\left[I+\frac{ds}{2}A(s_i)\right]\vec{y}_i := B_i\vec{y}_i. \tag{12}$$

Thus $\vec{y}_n$ is related to $\vec{y}_1$ as follows:

$$\vec{y}_n \simeq B_{n-1}B_{n-2}\cdots B_1\vec{y}_1 := \beta\vec{y}_1. \tag{13}$$

Equation 13 represents four equations in six unknowns. The unknowns are $\tilde{T}_1$, $\tilde{T}_n$, $\tilde{\phi}_1$, $\tilde{\phi}_n$, and $p_1$ and $q_1$, and the top endpoint boundary conditions provide $p_n$ and $q_n$.

### *B. Towfish Statics and Dynamics*

The two additional equations needed are found by looking at the towfish dynamics, and the relationship between the tension and angle at the connection point ($i = 1$). As with the cable, we write the full dynamic equations and linearize them with respect to a static configuration. The general equations of motion for the towfish in still water are

$$M\frac{D\vec{v}}{Dt} = \Sigma F = F_a + F_b + F_c + F_d + F_w \tag{14}$$

where the $a, b, c, d$, and $w$ denote respectively added mass, buoyancy, cable tension, drag, and weight terms. Note that this format is not necessarily accurate for streamlined bodies; in that case, it would be preferable to use the standard submarine equations of motion (e.g., [7]). Applying standard Euler angle manipulations [5], and using the cross product of the right-hand side with the appropriate radius vectors to get the moment equation, we obtain the following:

$$\begin{aligned} M\left(\frac{\partial U}{\partial t}-\frac{\partial\Phi}{\partial t}V\right) &= -M_{aP}\frac{\partial U}{\partial t} + B\sin\Phi + T_1\cos(\phi_1-\Phi) \\ &\quad -\frac{1}{2}\rho(C_{dP}A_P|U| + C_{dQ}A_Q|V|)U - W\sin\Phi \end{aligned} \tag{15}$$

$$\begin{aligned} M\left(\frac{\partial V}{\partial t}+\frac{\partial\Phi}{\partial t}U\right) &= -M_{aQ}\frac{\partial V}{\partial t} + B\cos\Phi + T_1\sin(\phi_1-\Phi) \\ &\quad -\frac{1}{2}\rho(C_{dP}A_P|U| + C_{dQ}A_Q|V|)V - W\cos\Phi \end{aligned} \tag{16}$$

$$\begin{aligned} J\frac{\partial^2\Phi}{\partial t^2} &= -r_{aP}M_{aQ}\frac{\partial V}{\partial t} + r_{aQ}M_{aP}\frac{\partial U}{\partial t} \\ &\quad + B(r_{bP}\cos\Phi - r_{bQ}\sin\Phi) \\ &\quad + T_1(r_{cP}\sin(\phi_1-\Phi) - r_{cQ}\cos(\phi_1-\Phi)) \\ &\quad -\frac{1}{2}\rho C_{d,t}A\frac{l^3}{32}\frac{\partial\Phi}{\partial t}\left|\frac{\partial\Phi}{\partial t}\right| \\ &\quad -\frac{1}{2}\rho\{C_{dP}A_P|U| + C_{dQ}A_Q|V|\}(r_{dP}V - r_{dQ}U). \end{aligned} \tag{17}$$

Note that the center of mass coincides with the weight center, so that there are no moments due to $W$. The rotational drag moment about the center of drag is approximated above as $-\frac{1}{2}\rho C_{d,t}A\frac{l^3}{32}\Phi'|\Phi'|$, where $A$ is the larger among $A_Q$ and $A_P$, and $l$ is the length of the towfish. For convenience, the rotational inertia $J$ includes both solid and added fluid inertia. However, we have allowed for the translational added mass and drag centers to be off the centroid. Finally, if there is a steady current $\mathcal{U}$, replace $U$ in the drag law by $U - \mathcal{U}\cos\Phi$, and $V$ by $V + \mathcal{U}\sin\Phi$. The static orientation of the towfish is the simultaneous solution to the static portion of the above equations.

The towfish dynamics may be found by performing the expansions in $\phi$, $\Phi$, and $T_1$, making the small angle assumption, and subtracting out the static parts. Unfortunately, there is no simple way to keep the coupled drag terms that appear in (15)–(17), using quasilinearization. As such, the formulation should not be expected to give accurate results when the dynamic pitching of the towfish is large, or when the drag forces are strongly coupled. The frequency-domain equations are as follows:

$$\begin{aligned} (-(M+M_{aP})\omega^2 + j\omega B_P)P &= -\tilde{T}_1\sin(\bar{\phi}_1-\bar{\Phi})(\tilde{\phi}_1-\tilde{\Phi}) \\ &\quad + \tilde{T}_1\cos(\bar{\phi}_1-\bar{\Phi}) \\ &\quad + (B-W)\cos\bar{\Phi}\tilde{\Phi}, \end{aligned} \tag{18}$$

$$\begin{aligned} (-(M+M_{aQ})\omega^2 + j\omega B_Q)Q &= \tilde{T}_1\cos(\bar{\phi}_1-\bar{\Phi})(\tilde{\phi}_1-\tilde{\Phi}) \\ &\quad + \tilde{T}_1\sin(\bar{\phi}_1-\bar{\Phi}) \\ &\quad - (B-W)\sin\bar{\Phi}\tilde{\Phi}, \end{aligned} \tag{19}$$

$$\begin{aligned} (-J\omega^2 + i\omega B_\Phi)\tilde{\Phi} &= -\omega^2(-r_{aP}M_{aQ}Q + r_{aQ}M_{aP}P) \\ &\quad - B(r_{bP}\sin\bar{\Phi}\tilde{\Phi} + r_{bQ}\cos\bar{\Phi}\tilde{\Phi}) \\ &\quad + \tilde{T}_1(r_{cP}\sin(\bar{\phi}_1-\bar{\Phi}) \\ &\quad - r_{cQ}\cos(\bar{\phi}_1-\bar{\Phi})) \\ &\quad + \tilde{T}_1\left\{r_{cP}\cos(\bar{\phi}_1-\bar{\Phi})(\tilde{\phi}_1-\tilde{\Phi})\right. \\ &\quad \left. + r_{cQ}\sin(\bar{\phi}_1-\bar{\Phi})(\tilde{\phi}_1-\tilde{\Phi})\right\} \\ &\quad + j\omega B_P P r_{dQ} - j\omega B_Q Q r_{dP}. \end{aligned} \tag{20}$$

As in the case of the cable, the linear dampers $B_P$, $B_Q$, and $B_\Phi$ are based on describing functions, and are to be found iteratively. Thus,

$$H(\omega)\begin{bmatrix}P\\Q\\\tilde{\Phi}\end{bmatrix} = G\begin{bmatrix}\tilde{T}_1\\\tilde{\phi}_1\end{bmatrix} \tag{21}$$

where $H(\omega)$ is a $3 \times 3$ invertible matrix. We also need a kinematic relationship between the motions of the towfish and the motions of the connection point; using the small-angle assumption again for $\tilde{\Phi}$ and $\tilde{\phi}_1$, the formula is

$$\begin{bmatrix} p_1 \\ q_1 \end{bmatrix} = \begin{bmatrix} \cos(\bar{\phi}_1 - \bar{\Phi}) & \sin(\bar{\phi}_1 - \bar{\Phi}) & -r_{cQ}\cos(\bar{\phi}_1 - \bar{\Phi}) + r_{cP}\sin(\bar{\phi}_1 - \bar{\Phi}) \\ -\sin(\bar{\phi}_1 - \bar{\Phi}) & \cos(\bar{\phi}_1 - \bar{\Phi}) & r_{cQ}\sin(\bar{\phi}_1 - \bar{\Phi}) + r_{cP}\cos(\bar{\phi}_1 - \bar{\Phi}) \end{bmatrix} \begin{bmatrix} P \\ Q \\ \bar{\Phi} \end{bmatrix} := R \begin{bmatrix} P \\ Q \\ \bar{\Phi} \end{bmatrix}. \tag{23}$$

### C. Transfer Matrices

Breaking the matrix $\beta$ of (13) into $2 \times 2$ blocks numbered $\beta_{11}$, $\beta_{12}$, $\beta_{21}$, and $\beta_{22}$, the relationships between the top point motions and the state of the cable are [1], [8]

$$\begin{bmatrix} P \\ Q \\ \bar{\Phi} \end{bmatrix} = H^{-1}G(\beta_{21} + \beta_{22}RH^{-1}G)^{-1} \begin{bmatrix} p_n \\ q_n \end{bmatrix} := \Sigma\vec{u} \tag{23}$$

$$\vec{y}_1 = \begin{bmatrix} (\beta_{21} + \beta_{22}RH^{-1}G)^{-1} \\ RH^{-1}G(\beta_{21} + \beta_{22}RH^{-1}G)^{-1} \end{bmatrix} \vec{u} := \Gamma\vec{u} \tag{24}$$

$$\vec{y}_i = \beta_i\Gamma\vec{u}\ , \text{ where } \beta_i := B_{i-1}B_{i-2}\cdots B_1,\ i = 2, 3, \cdots, n \tag{25}$$

$$\begin{bmatrix} \hat{T}_n \\ \hat{\phi}_n \end{bmatrix} = [\beta_{11}\ \ \beta_{12}]\Gamma\vec{u} := \Delta\vec{u}. \tag{26}$$

## III. Drag Linearization

The response of the above system to purely sinusoidal excitations may be computed using a simple iteration scheme which accounts for the drag nonlinearities in the cable and towfish models [16]. A bisection approach is helpful in speeding up the convergence.

The linearization of drag is generally based on equal dissipation [17]. Let $v(s,t) = \zeta(s)\sin(\lambda t)$ be a generic velocity for the cable; it represents $\frac{dp_i}{dt}$, $\frac{dq_i}{dt}$, $\frac{dP}{dt}$, $\frac{dQ}{dt}$, and $\frac{d\Phi}{dt}$. Suppose for simplicity that the scaling factors (e.g., $0.5\rho C_d d$) are unity. A steady horizontal current $\mathcal{U}$ exists, which is assumed to be uniform with depth, although this restriction can easily be removed. Note also that $B_\Phi$ is independent of $\mathcal{U}$. There are three distinct cases:

1. $|\mathcal{U}| = 0 \longrightarrow b_v(s) = \frac{8}{3\pi}|\zeta(s)|$.
2. $|\mathcal{U}| \geq |\zeta(s)| \longrightarrow b_v(s) = 2|\mathcal{U}|$.
3. $|\zeta(s)| > |\mathcal{U}| > 0 \longrightarrow$

$$b_v(s) := \frac{4}{\pi\zeta(s)}\left[-\mathcal{U}|\zeta(s)|\sin^{-1}\left(\frac{-\mathcal{U}}{|\zeta(s)|}\right) + \frac{1}{3}(\mathcal{U}^2 + 2\zeta^2(s))\sqrt{1 - \frac{\mathcal{U}^2}{\zeta^2(s)}}\ \right].$$

In the limit as $\zeta(s) \to \mathcal{U}$, and $\mathcal{U} \to 0$, the simpler formulas of Cases 2 and 1, respectively, are recovered.

Sometimes a statistical description of the response is more appropriate than direct harmonic analysis. Since the present method uses linearization, the usual spectral analysis tools can be employed. The response-amplitude operator (RAO) of a physical system relates the input spectrum to the output spectrum through the relation $\Phi_{\vec{y}_1\vec{y}_1}(\omega) = \Gamma(-\omega)\Phi_{\vec{u}\vec{u}}\Gamma^T(\omega)$, where our transfer matrix $\Gamma(\omega)$ is used as an example. If $\Phi_{\vec{u}\vec{u}}$ is a one-sided double-amplitude spectrum, then the amplitude covariance of the output is given by

$$\sigma^2_{\vec{y}_1} = \frac{1}{2\pi}\int_0^\infty \Gamma(-\omega)\Phi_{\vec{u}\vec{u}}(\omega)\Gamma^T(\omega)d\omega.$$

With regard to equivalent linearization, now let $v = \zeta(t)\cos(\omega t + \delta(t))$, where $\zeta(t)$ and $\delta(t)$ are independent narrow-band gaussian processes. Then we have [20]

$$b_v = \sqrt{\frac{8}{\pi}}\sigma_\zeta\left\{\frac{|\mathcal{U}|}{\sigma_\zeta}\sqrt{\frac{\pi}{2}}\ \text{erf}\left(\frac{|\mathcal{U}|}{\sqrt{2}\sigma_\zeta}\right) + \exp\left(-\frac{\mathcal{U}^2}{2\sigma^2_\zeta}\right)\right\}.$$

## IV. Applications

### A. Incorporation of a Heave Compensator

The core equations of Section II-C can be appended to include a passive heave compensator in the analysis. Passive compensators normally use gas cylinders as compliant elements; consistent with the our approach, any pneumatic and geometric nonlinearities should be linearized about a mean position. We model the compensator as a spring of stiffness $k_{\text{comp}}$ in parallel with a dashpot of damping $b_{\text{comp}}$, placed between the heaving vessel and the cable nodal point numbered $n$. The compensator also has an apparent mass $m_{\text{comp}}$, that moves with the $n$th node of the cable.

Since lateral motions imparted to a submerged cable are attenuated very rapidly, we consider only the case in which the vessel heave is exactly aligned with the static cable configuration. Let the heaving motion of the vessel be denoted as $D(t)$. Then a little manipulation and the definition of $\Delta$ give

$$p_n(\omega) = \frac{j\omega b_{\text{comp}} + k_{\text{comp}}}{\Delta_{11} - \omega^2 m_{\text{comp}} + j\omega b_{\text{comp}} + k_{\text{comp}}} D(\omega) := Z(\omega)D(\omega). \tag{27}$$

The calculation of $Z(\omega)$ must be inside the iteration loop since it involves $\Delta$, which in turn depends on $\beta$.

### B. Example 1: Heave Compensation Case Study

During towing at relatively high speeds and in large waves, the motions transmitted down a long tow cable are almost exclusively axial, and may excite significant modes of the towfish and of the cable. Towfish modes are generally undesirable since they tend to smear acoustic or optical images so obtained. At the same time, the tensions at both ends of the cable must be monitored to ensure that snap loading does not occur, and that the ultimate strength of the cable is not surpassed. The former occurs when the dynamic tension amplitude exceeds the static tension, and the latter when the sum of the static and dynamic tensions exceeds the cable's ultimate strength.

The stability of the towfish is largely dependent on its physical parameters, and upon the speed at which it is towed [2]–[4], [11]. Chapman in [3] provided a comprehensive

design analysis for the Mk 3 sonar towfish, illustrating pitch responses to cyclic disturbances at the towpoint and to disturbances in the water, such as turbulence. The requirement that both responses be small is conflicting, since the first is alleviated by aligning the towpoint with the mass and aerodynamic centers, while the second is reduced with large stabilizing fins far aft.

Another way to reduce the motions and tensions in a towed system is through passive heave compensation. A bobbing-crane design, for example, has an apparent stiffness and damping, which can be utilized for the best performance. It is well known that if the waves are small, or if the range (distance between the stops) of the compensator is very large, the most effective approach minimizes the system's natural frequency. This can be achieved in practice by making the apparent stiffness and damping in the compensator small. In contrast, when the vessel motions exceed the allowable travel of the compensator, the compensator must be "tightened up" in such a way that the travel is acceptable *and* the motions of the top of the cable are reduced. Otherwise, one would simply lock the compensator in high seas.

Here, we will address this latter compensation tuning problem. To set the stage, the frequency response of the system in Table II was computed using the quasilinear method. Noteworthy is the fact that our model has no lift, in contrast to the Mk 3 type of design; the application is slow, deep towing. The top of the cable was excited by a one-meter sinusoid, and $\mathcal{U} = 0$ uniformly. The results are shown in Fig. 2. The heave ($Q(\omega)$) has a damped natural frequency of 0.90 rad/s, with an amplification of 5.25 dB at that point. Hence, we expect this system to resonate in heave for sea states 3 or 4. The pitching response increases with frequency, but not enough that the small angle assumption of Section II-B is invalid. Finally, the dynamic tensions reach their first peak at 1.19 rad/s.

A preliminary study of the purely linear dynamics is illuminating. Four transfer functions are relevant:

- The ratio of towfish heave to vessel heave, $\frac{p_1(\omega)}{D(\omega)}$. Note that $p_1 = Q$ if the towfish has no pitch dynamics and $\bar{\Phi} = 0$.
- The ratio of cable top heave in the vessel frame to vessel heave, $\frac{R(\omega)}{D(\omega)}$. This is the motion seen by an observer on the vessel.
- The ratio of dynamic tension at the towfish to vessel heave motion, $\frac{T_1(\omega)}{D(\omega)}$.
- The ratio of dynamic tension at the surface to vessel heave motion, $\frac{T_n(\omega)}{D(\omega)}$.

These functions can be found as solutions to the eigenvalue problem, as outlined in the appendix. We computed them for sea state 5 and 6 conditions, considering only the response at the peak frequency $\omega_0$ and linearizing for drag uniformly at the velocity $D_{1/3}\omega_0$. The responses were found for a large range of values for $k_{\text{comp}}$ and $b_{\text{comp}}$; results are shown in Figs. 3 and 4 for sea state 6 conditions.

As expected, the dynamic tensions and heave of the towfish are very small when the stiffness and damping in the compensator are small. As $k_{\text{comp}}$ is increased, the responses tend to peak strongly, whereas when $b_{\text{comp}}$ is increased, they grow monotonically toward the locked-compensator result. The relative motion of the compensator, $R(\omega)$, has a somewhat different dependence on $k_{\text{comp}}$ and $b_{\text{comp}}$. Here, the locked compensator admits no relative motion, while low stiffness and damping cause all of the vessel motion to be taken up. Of special interest is the fact that the same peak is apparent in the relative response, at the same value of $k_{\text{comp}}$ which maximizes the other three responses. A similar computation was made for sea state 5 conditions, and the surface shapes are similar, although because of the lower linearization speed, the ridge is somewhat higher.

Several observations can be made. First, there exists a critical stiffness, $k_{\text{crit}}$, above which amplification of deflections and tensions occurs; this stiffness can be determined

TABLE II
NOMINAL PARAMETERS FOR COMPENSATOR ANALYSIS

| | |
|---|---|
| $L$ | 4000 m |
| $d$ | 0.0173 m |
| $w_o$ | 8.14 N/m |
| $m$ | 1.04 kg/m |
| $m_a$ | 0.20 kg/m |
| $\rho$ | 1025 kg/m$^3$ |
| $C_d$ | 1.6 |
| $C_t$ | 0.01 |
| $E$ | $42 \times 10^9$ N/m$^2$ |
| $W$ | 3920 N |
| $B$ | 780 N |
| $M$ | 400 kg |
| $M_{aP}$ | 500 kg |
| $M_{aQ}$ | 500 kg |
| $J$ | 280 kg-m$^2$ |
| $C_{d,t}$ | 2 |
| $A_P$ | 0.25 m$^2$ |
| $A_Q$ | 1.0 m$^2$ |
| $l$ | 2.0 m |
| $r_{aP}$ | -0.05 m |
| $r_{aQ}$ | 0.0 m |
| $r_{bP}$ | 0.0 m |
| $r_{bQ}$ | 0.02 m |
| $r_{cP}$ | 0.0 m |
| $r_{cQ}$ | 0.8 m |
| $r_{dP}$ | -0.05 m |
| $r_{dQ}$ | 0.0 m |
| $m_{comp}$ | 530 kg |

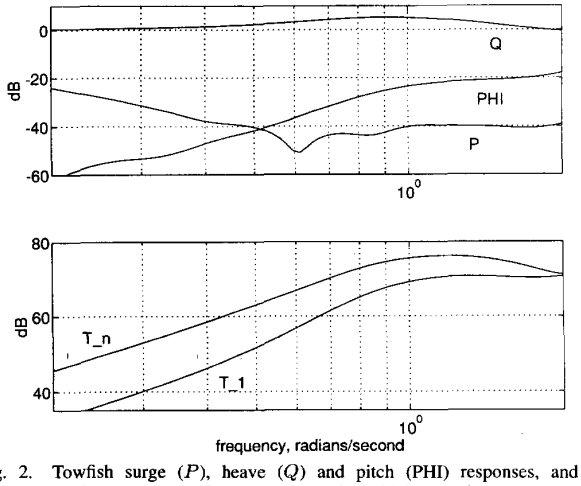


Fig. 2. Towfish surge ($P$), heave ($Q$) and pitch (PHI) responses, and endpoint tensions (newtons) for a one-meter sinusoidal excitation.

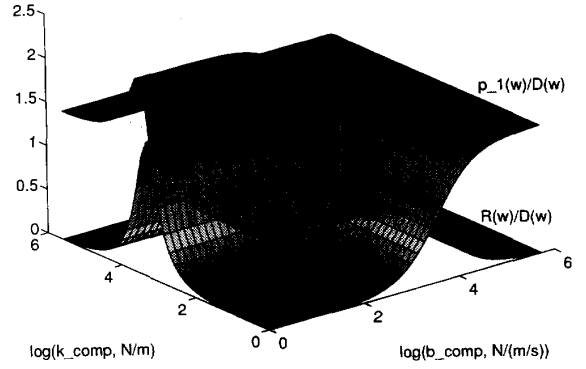


Fig. 3. Towfish heave ($p_1(\omega)$) and compensator ($R(\omega)$) amplitudes as a function of $k_{\rm comp}$ and $b_{\rm comp}$, at the most probable frequency in sea state 6.

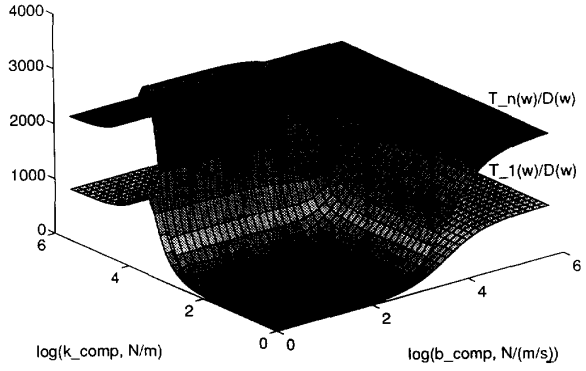


Fig. 4. Endpoint tension ($T_1(\omega)$ and $T_n(\omega)$) amplitudes as a function of $k_{\rm comp}$ and $b_{\rm comp}$, at the most probable frequency in sea state 6.

beforehand and should be avoided. In Fig. 3, $k_{\rm crit}$ is the largest value of $k_{\rm comp}$ for which $|p_1(\omega)|$ is less than the locked-compensator value, for all values of $b_{\rm comp}$. Furthermore, one sees that there is a stiffness solution and a damping solution. In the first, we assume that the damping is small and the stiffness should be tuned; in the second, the stiffness is small and the damping is tuned. Clearly, the stiffness solution can be expected to yield the larger values of $p_1$, $T_1$, and $T_n$. Basic rules for tuning in high seas are as follows:

- $\min(k_{comp}) < k_{crit}$. Increase the apparent damping as necessary to constrain the compensator motion.
- $\min(k_{\rm comp}) \geq k_{\rm crit}$. Lock the compensator.

These rules are quite distinct from current practice. Existing compensators are usually designed to minimize overall fluid losses (hence $b_{\rm comp}$), while the stiffness is adjustable online by changing the air volume. Our view is that a design effort which concentrates on reducing the minimum apparent stiffness, while allowing tunable damping, should lead to better constrained performance.

Let us now consider the statistical aspects of this compensation scheme. The Monterey Bay Aquarium Research Institute is acquiring a SWATH (Small Waterplane Area—Twin Hull) vessel, and we applied its RAO to the Bretschneider spectrum [18], [6]. The heave spectrum at the deck in sea state 6 is given

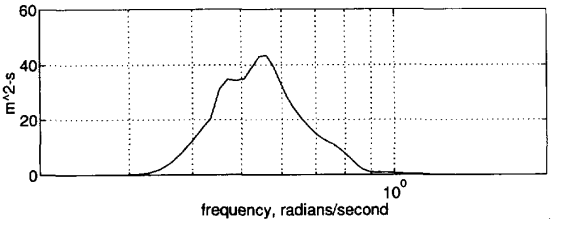


Fig. 5. Spectrum of SWATH vessel heave motions in sea state 6.

TABLE III
TUNED VALUES FOR $k_{\rm comp}$ AND $b_{\rm comp}$, BASED ON LINEAR ANALYSIS

| | | sea state 5 | sea state 6 |
|---|---|---|---|
| stiffness-tuned | $k_{comp}$ | 6410 N/m | 7020 N/(m/s) |
| | $b_{comp}$ | 100 N/(m/s) | 100 N/(m/s) |
| damping-tuned | $k_{comp}$ | 100 N/m | 100 N/m |
| | $b_{comp}$ | 3160 N/(m/s) | 7150 N/(m/s) |
| | $k_{crit}$ | 1600 N/m | 1510 N/m |

TABLE IV
RESULTS OF STIFFNESS- AND DAMPING-TUNED HEAVE COMPENSATION STRATEGIES

| | | locked comp. | tuned stiffness | tuned damping |
|---|---|---|---|---|
| sea state 5 | $H_{1/3}$ | 3.23 | 3.23 | 3.23 |
| | $D_{1/3}$ | 2.99 | 2.99 | 2.99 |
| | $p_{n,1/3}$ | 2.99 | 3.28 | 1.28 |
| | $R_{1/3}$ | 0.00 | 1.74 | 2.21 |
| | $Q_{1/3}$ | 4.81 | 4.99 | 2.32 |
| | $R_{1/1000}$ | 0.00 | 3.24 | 4.11 |
| | $T_{1,1/1000}$ | 5.18 | 5.38 | 1.42 |
| | $\bar{T}_1$ | 3.14 | 3.14 | 3.14 |
| | $T_{n,1/1000}$ | 10.62 | 10.47 | 4.51 |
| | $\bar{T}_n$ | 35.70 | 35.70 | 35.70 |
| sea state 6 | $H_{1/3}$ | 4.99 | 4.99 | 4.99 |
| | $D_{1/3}$ | 5.25 | 5.25 | 5.25 |
| | $p_{n,1/3}$ | 5.25 | 5.53 | 3.47 |
| | $R_{1/3}$ | 0.00 | 2.07 | 2.13 |
| | $Q_{1/3}$ | 7.02 | 7.25 | 5.06 |
| | $R_{1/1000}$ | 0.00 | 3.84 | 3.95 |
| | $T_{1,1/1000}$ | 7.77 | 8.09 | 4.08 |
| | $\bar{T}_1$ | 3.14 | 3.14 | 3.14 |
| | $T_{n,1/1000}$ | 13.55 | 13.68 | 8.80 |
| | $\bar{T}_n$ | 35.70 | 35.70 | 35.70 |

in Fig. 5. The significant heave height of the SWATH deck in sea state 6 is 5.25 m, while the available compensator travel is 4.0 m. Setting the 1000th highest compensator response (height) to be 4.0 m gives the requirement that $|R(\omega)/D(\omega)| \leq 0.41$. As described above, there are two solutions, depending on whether the compensator stiffness or damping is tuned. The tuned values are listed in Table III, and results are given in Table IV, for sea states 5 and 6. We considered lower sea states also, but found that the SWATH motions then are small enough that the compensator does not have to be constrained.

In the sea state 6 runs, the compensator motion constraint has been closely matched, while for the sea state 5 runs, the error is larger. This difference is due to the fact that the sea state 5 runs involve frequencies closer to the system's first natural mode, making the preliminary calculations less accurate. Nevertheless, the main points are still clear in both cases: effective compensation is achieved by tuning $b_{\rm comp}$, and locking the compensator is better than tuning $k_{\rm comp}$. To see

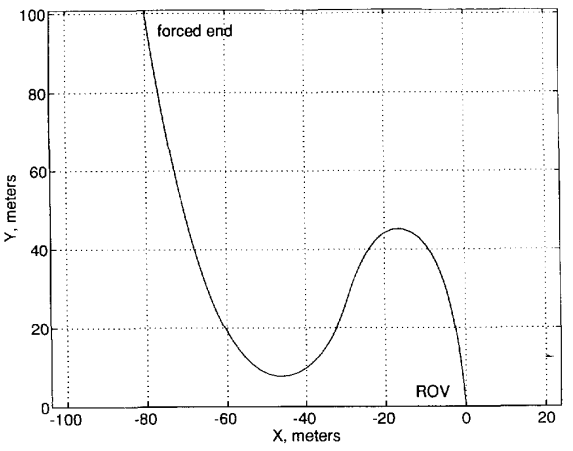


Fig. 6. Static $S$-shape configuration for Example 2.

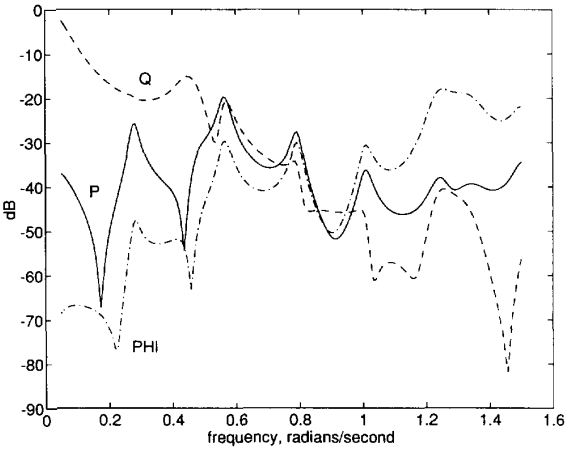


Fig. 7. ROV frequency response through an $S$-shaped cable: surge ($P$), heave ($Q$), and pitch ($\Phi$).

this, compare the towfish significant heave heights ($Q_{1/3}$), and the extreme dynamic tensions at the towfish ($T_{1,1/1000}$) and at the surface ($T_{n,1/1000}$).

### C. Example 2: Transferred Motions Through a Short S-Shape

Many ROV applications employ a length of buoyant tether near the ROV; if the remainder of the tether is heavy in water, then an "$S$-shape" is formed. This $S$-shape will isolate the ROV from the heave motions of the surface vessel to some extent, while at the same time give the ROV an unobstructed view of the seafloor. Since the $S$-shape involves large static curvatures, the analysis of its dynamic response is an interesting application of our method.

This example involves a system modified slightly from Table II. The ROV has the same parameters given, except that the buoyancy is increased so that the in-water weight of the towfish is 500 N. Note that this could as easily be achieved with thrusters as with actual floatation. In addition, the 75 m of cable nearest the ROV is floated to achieve a net buoyancy of 10.2 N/m. Since we are most interested in the response of the $S$-shape formed, the depth of the ROV is taken to be only 100 m. The static shape with $\mathcal{U} = 0.2$ m/s is given in Fig. 6. The static ROV pitch angle is 8.0°, and the static tensions are $T_1 = 530$ N and $T_n = 840$ N. The cable length is 205 m.

The frequency response was computed using the matrix method for frequencies between 0.05 and 1.50 rad/s, with a one-meter axial excitation. The results are shown in Figs. 7 and 8. This range of frequencies appears to include a number of distinct resonant modes, which are irregularly spaced. (We verified that there are no other peaks below 0.05 rad/s.) Overall, the ROV heave ($Q$) cutoff occurs at less than 0.05 rad/s, and reaches $-40$ dB by 0.80 rad/s. In contrast, the ROV surge ($P$) does not show any significant rolloff in the range, although it does have several zeros at low frequencies. The dynamic pitch angle ($\tilde{\Phi}$) appears to rise with frequency as in Example 1, reaching six degrees at 1.25 rad/s. Note that these values are not necessarily small from an operational point of view: $-30$ dB in $Q$ or $P$ means a six-centimeter peak-to-peak oscillation. Perhaps more importantly, $-30$ dB

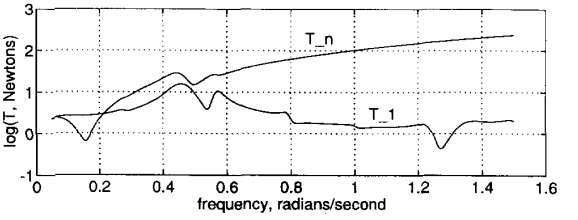


Fig. 8. Dynamic tensions in an $S$-shaped cable at the ROV ($T_1$) and at the excited end ($T_n$).

in $\tilde{\Phi}$ corresponds with a 3.6° peak-to-peak oscillation. If the ROV is gathering visual or sonar data, this motion may be prohibitive.

The dynamic tensions have relatively weak peaks, with no unloading of the cable at either end. One should note, however, that while the tension at the ROV stays low throughout the wave regime, tension at the forced end is increasing with frequency.

We computed the mode shapes for peaks at the lower frequencies; the cable deflections are shown in Fig. 9. The figure gives two dynamic shapes for each frequency, 180° out of phase and magnified by a factor of five. The first peak in surge ($P$) occurs near 0.280 rad/s, and here the cable essentially swings in a counterclockwise manner, with very little deformation. The heave $Q$ peaks next at 0.435 rad/s. The buoyant part of the cable moves vertically, while the heavy portion swings right and left of the static curve. The peak near 0.550 rad/s is the strongest; here, the arc of floated cable and the heavy cable swing from side to side. The modes at higher frequencies show increasing regularity, although admittedly they are harder to describe with words. Connections with the modal analysis of single-span cables [13], [21], [23] would be an interesting topic for further study.

### D. Computational Considerations

A few words are in order about the accuracy and computational cost of our approach. The iteration test condition in

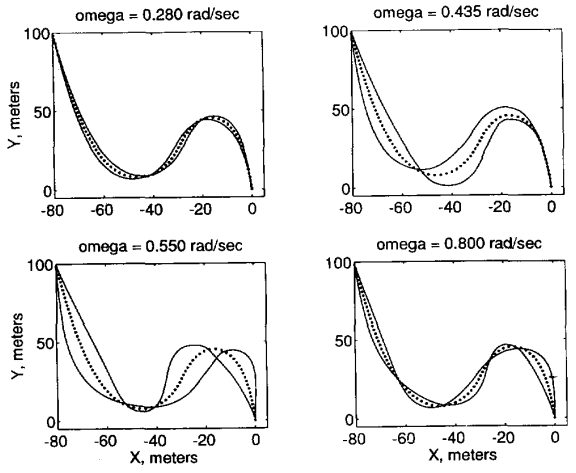


Fig. 9. First four modes for an $S$-shaped cable. *Dotted line:* static configuration, *solid lines:* deflections with 90 and 270° phase lag.

the examples was

$$\text{TOL} \geq \frac{\int_0^L \delta p(s)^2 + \delta q(s)^2 ds}{L(p_n^2 + q_n^2)},$$

where $\delta p(s)$ and $\delta q(s)$ are the respective differences in $p$ and $q$ values between iterations $k$ and $k+1$. A value of TOL $= 0.0001$ gave good accuracy and required around six iterations to converge at each frequency. Note that the number of iterations required in the harmonic analysis can be reduced by using the final damping coefficients from the previous frequency calculation. In the case of random excitation, this is not possible, since the entire response spectrum has to be computed before new damping coefficients can be found.

The accuracy of the method was checked in the context of heave compensation. A nonlinear time-domain model was constructed, including quadratic drag, and pneumatic and geometric nonlinearities associated with a bobbing crane compensator. For a range of compensator parameters (e.g., air volume, isentropic coefficient), we computed the responses of several different cable lengths to random waves, in different sea states; see [9]. The same conditions were then employed in the equivalent linearization algorithm. Results are shown in Table V; the RMS errors are all under fifteen percent. On an HP 705 workstation running Matlab Version 4.0 software [19], the simulations required over two hours each of CPU time, while the equivalent linearization approach took approximately 110 s. In the simulation, we used approximately twenty wave crests, twenty nodes, and an adaptive time-step Runge–Kutta integrator. In the frequency-domain method, we used forty frequencies, twenty-one nodes, and five iterations.

A breakdown of the computational cost for analysis of the $S$-shape in Example 2, with $n = 83$, is given in Table VI. The largest amount of CPU time is spent calculating the $\beta$ matrix, which involves a complex $4 \times 4$ inverse and multiply at each node. These two operations alone require 1640 FLOPS (Floating Point Operations). One hundred frequency points took 1160 s of CPU time.

TABLE V
COMPARISON OF NONLINEAR AND EQUIVALENT LINEARIZATION ANALYSES

| | | | | |
|---|---|---|---|---|
| | air volume, $m^3$ | 0.283 | 0.057 | 0.028 |
| | isentropic coefficient | 1.22 | 1.44 | 1.00 |
| | cylinder fluid drag, $kN/(m/s)^2$ | 28.69 | 9.56 | 9.56 |
| | depth, m | 2500 | 4000 | 2000 |
| | Seastate | 4 | 5 | 6 |
| Simulation | Crests in Record | 19 | 23 | 18 |
| | RMS $D(t)$, m | 0.43 | 0.74 | 1.28 |
| | RMS $p_n(t)$, m | 1.06 | 1.10 | 1.63 |
| | RMS $Q(t)$, m | 1.27 | 1.75 | 1.81 |
| | maximum $Q(t)$ height, m | 4.8 | 6.5 | 10.0 |
| | RMS $R(t)$, m | 1.01 | 0.50 | 0.52 |
| Equivalent | $\sigma_D$, m | 0.39 | 0.75 | 1.31 |
| Linearization | $\sigma_{p_n}$, m | 0.97 | 1.12 | 1.63 |
| | $\sigma_Q$, m | 1.19 | 2.02 | 1.82 |
| | $Q_{1/10}$, m | 6.1 | 10.3 | 9.3 |
| | $\sigma_R$, m | 0.85 | 0.54 | 0.45 |

TABLE VI
FLOATING POINT OPERATIONS REQUIRED FOR EXAMPLE 2

| | $n = 83$ | normalized |
|---|---|---|
| compute $A(s)$, $\beta$ | 201600 | $2430n$ |
| compute other transfer matrices | 4400 | 4400 |
| get $\vec{y}$ along length | 11300 | $136n$ |
| update damping coefficients | 3800 | $46n$ |
| compute error norm | 6000 | $72n$ |
| Total FLOPS per iteration | 227100 | $2684n+4400$ |

## V. CONCLUSION

An extension of Bliek's matrix method for mooring system dynamic analysis has been directly extended to address the behavior of towed vehicle systems. The tool should be useful for a variety of analyses, two examples of which were discussed. We examined a fundamental problem in passive heave compensation, an oceanographic application that has not really received enough critical attention. The second example revealed a complex dynamic response for $S$-shaped cables; this will be the subject of future work.

## APPENDIX

The linear governing equation for the damped axial motion of a string is

$$m\frac{\partial^2 p(s,t)}{\partial t^2} + b_p\frac{\partial^2 p(s,t)}{\partial t} = EA\frac{\partial^2 p(s,t)}{\partial s^2}. \tag{28}$$

The top and bottom boundary conditions are, respectively

$$p(s=L,t) = p_n(t), \tag{29}$$

$$(M + M_{aQ})\frac{\partial^2 Q(t)}{\partial t^2} + B_Q\frac{\partial Q(t)}{\partial t} = EA\frac{\partial p(s=0,t)}{\partial s}. \tag{30}$$

Then using the Laplace transform to replace time with frequency, separation of variables gives

$$\frac{p_1(\omega)}{p_n(\omega)} = \frac{\gamma(\omega)}{\gamma(\omega)\cosh(\gamma(\omega)L) + \Gamma(\omega)^2\sinh(\gamma(\omega)L)} \tag{31}$$

where

$$\gamma(\omega) := \sqrt{\frac{-m\omega^2 + j\omega b_p}{EA}}, \text{ and } \Gamma^2(\omega) := \frac{-(M + M_{aQ})\omega^2 + j\omega B_Q}{EA}.$$

In addition,

$$\frac{T_1(\omega)}{p_n(\omega)} = \frac{EA\gamma\left(\gamma\sinh(\gamma L) + \Gamma^2\cosh(\gamma L)\right)}{\gamma\cosh(\gamma L + \Gamma^2\sinh(\gamma L)}, \quad (32)$$

$$\frac{T_n(\omega)}{p_n(\omega)} = \frac{EA\gamma\Gamma^2}{\gamma\cosh(\gamma L) + \Gamma^2\sinh(\gamma L)}. \quad (33)$$

Finally, note that

$$\frac{R(\omega)}{D(\omega)} = \frac{p_n(\omega)}{D(\omega)} - 1, \quad (34)$$

and apply Section IV-A; the transfer functions can now be easily constructed.

## REFERENCES


[1] A. Bliek, "Dynamic Analysis of Single Span Cables," Ph.D. dissertation, Massachusetts Institute of Technology, 1984.

[2] D. A. Chapman, "Effects of ship motion on a neutrally-stable towed fish," *Ocean Eng.*, vol. 9, pp. 189–220, 1982.

[3] D. A. Chapman, "The adjustment of fin size to minimise the ship induced pitching motion of a towed fish," *Ocean Eng.*, vol. 11, pp. 23–64, 1984.

[4] D. A. Chapman, "A study of the ship induced roll-yaw motion of a heavy towed fish," *Ocean Eng.*, vol. 11, pp. 627–654, 1984.

[5] S. H. Crandall, D. C. Karnopp, E. F. Kurtz, Jr., and D. C. Pridmore-Brown, *Dynamics of Mechanical and Electromechanical Systems*. Malabar, FL: Krieger Publishing, 1968.

[6] O. M. Faltinsen, *"Sea Loads on Ships and Offshore Structures*. New York: Cambridge University Press, 1990.

[7] J. Feldman, "DTNSRDC Revised Standard Submarine Equations of Motion," Tech. Rep., David W. Taylor Naval Ship Research and Development Center, 1979.

[8] M. A. Grosenbaugh and M. S. Triantafyllou, "A Fast Numerical Method for Dynamic Analysis of Buoy-Cable Interactions," unpublished report, 1992.

[9] F. S. Hover, "Passive Heave Compensation With A Bobbing Crane," unpublished manuscript, Monterey Bay Aquarium Research Institute, 1993.

[10] C. T. Howell, "Investigation of the Dynamics of Low-Tension Cables," Ph. D. dissertation, Massuchusetts Institute of Technology/Woods Hole Oceanographic Institution, 1992.

[11] R. M. Hubbard, "Hydrodynamic design of a sonar towfish for minimal image-smearing in heavy seas," in *Proc. OCEANS'89*, Seattle, WA, 1981.

[12] H. M. Irvine, *Cable Structures*. Cambridge, MA: MIT Press, 1981.

[13] H. M. Irvine and T. K. Caughey, "The linear theory of free vibrations of a suspended cable," *Proc. Royal Society of London*, vol. A341, pp. 299–315, 1974.

[14] K. P. Kerney, "Small-Perturbation Analysis of Oscillatory Tow-Cable Motion," NDRDC Rep. 3430, 1971.

[15] N. Kryloff and N. Bogoliubof, *Introduction to Nonlinear Mechanics*. Princeton, NJ: Princeton University Press, 1947.

[16] A. K. Malhotra and J. Penzien, "Nondeterministic analysis of offshore structures," *J. Eng. Mech. Division, Proc. ASCE*, vol. 96, pp. 985–1003, 1970.

[17] J. R. Paulling, "Frequency domain analysis of OTEC CW pipe and platform dynamics," in *Proc. Offshore Technology Conf.*, 1979.

[18] T. Sarpkaya and M. Isaacson, *Mechanics of Wave Forces on Offshore Structures*. New York: Van Nostrand Reinhold, 1981.

[19] The Mathworks, Inc. MATLAB numeric computation and visualization software, 1992.

[20] M. S. Triantafyllou, "Preliminary design of mooring systems," *J. Ship Res.*, vol. 26, pp. 25–35, 1982.

[21] M S. Triantafyllou, "The dynamics of taut inclined cables," *Q. J. Mech. App. Math.*, vol. 37, pp. 421–440, 1984.

[22] M. S. Triantafyllou, "Dynamics of cables, towing cables, and mooring systems," *Shock and Vibration Dig.*, vol. 23, pp. 3–8, 1991.

[23] M. S. Triantafyllou and L. Grinfogel, "Natural frequencies and modes of inclined cables," *ASCE J. Structural Eng.*, vol. 112, pp. 139–148, 1986.


**Franz S. Hover** received the B.S.M.E. degree from Ohio Northern University in 1987. He proceeded to the Massachusetts Institute of Technology/Woods Hole Oceanographic Institute Joint Program in Oceanic Engineering, where he received the M.S. degree in 1989 and Sc.D. degree in 1993.

He is currently a postdoctoral fellow at the Monterey Bay Aquarium Research Institute. His research interests include dynamics of ocean systems and nonlinear control system design.

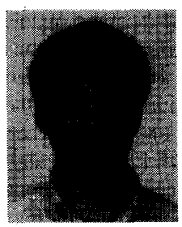

**Mark A. Grosenbaugh** received the B. S. and M. S. degrees from Stanford University in 1976 and 1983, respectively, and the Ph.D. degree from the University of California, Berkeley, in 1987.

Since 1987, he has been at the Woods Hole Oceanographic Institution, Woods Hole, MA, where he is currently an Associate Scientist in the Department of Applied Ocean Physics and Engineering. He is also a Lecturer in the Department of Ocean Engineering at the Massachusetts Institute of Technology, Cambridge.

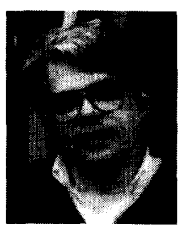

**Michael S. Triantafyllou** graduated from the National Technical University of Athens, Greece in 1974, and received the Sc.D. degree from the Massachusetts Institute of Technology in 1979.

He joined the MIT faculty in 1979, and is currently a Professor of Ocean Engineering and Director of the Ocean Engineering Testing Tank Facility. He teaches and conducts research on the mechanics of cables, and on the dynamics and control of shear flows.